Spin-Wave frequency division multiplexing in an yttrium iron garnet microstripe magnetized by inhomogeneous field.

Zhizhi Zhang<sup>1,2</sup>, Michael Vogel<sup>1</sup>, José Holanda<sup>1</sup>, M. Benjamin Jungfleisch<sup>3</sup>, Changjiang Liu<sup>1</sup>, Yi Li<sup>1,4</sup>, John E. Pearson<sup>1</sup>, Ralu Divan<sup>5</sup>, Wei Zhang<sup>4</sup>, Axel Hoffmann<sup>1,6</sup>, Yan Nie<sup>2,\*</sup>, and Valentyn Novosad<sup>1,†</sup>

- <sup>1</sup> Materials Science Division, Argonne National Laboratory, Argonne, IL 60439, USA
- <sup>2</sup> School of Optical and Electronic Information, Huazhong University of Science and Technology, Wuhan 430074, China
- <sup>3</sup> Department of Physics and Astronomy, University of Delaware, Newark, DE 19716, USA
- <sup>4</sup> Department of Physics, Oakland University, Rochester, MI 48309, USA
- <sup>5</sup> Center for Nanoscale Materials, Argonne National Laboratory, Argonne, IL 60439, USA
- <sup>6</sup> Department of Materials Science and Engineering, University of Illinois at Urbana-Champaign, Urbana, IL 61801, USA

## **Abstract**

Spin waves are promising candidates for information processing and transmission in a broad frequency range. In the realization of magnonic devices, the frequency related division of the spin waves is a critical function for parallel information processing. In this work, we demonstrate a proof-of-concept spin-wave frequency division multiplexing method by magnetizing a homogenous magnetic microstripe with an inhomogeneous field. The symmetry breaking additional field is introduced by a permalloy stripe simply placed in lateral proximity to a yttrium iron garnet waveguide. Spin waves with different frequencies can propagate independently, simultaneously and separately in space along the shared waveguide. This work demonstrates one potential way for parallel information transmission and processing in magnonics.

Next-generation computation concepts require parallel data processing and transmission simultaneously in a single, shared data-bus to achieve high efficiency and compact integration. In such systems, frequency division multiplexers (FDMs) play an important role in the separation of multiple signals encoded in different frequencies.<sup>1</sup> The FDM concept is also important in the emerging field of magnonics.<sup>2-7</sup> In magnonic circuits, spin waves (SWs) and their quasiparticles, i.e. magnons, can encode the information in their amplitude<sup>8, 9</sup> or phase<sup>10, 11</sup> in a broad frequency range.<sup>12, 13</sup> An important concept in magnonics is the logic operation, which relies on wave-based interactions, especially interference<sup>14</sup>, and the control of SW flows<sup>6, 7</sup>. It paves a way to the wave-based computation.<sup>15, 16</sup> Interference requires the coherent SWs to have the same or nearly the same frequency. Therefore in parallel data processing, the FDM is a

crucial component in realizing practical magnonic circuits.<sup>17</sup>

In the context of improving the magnonic signal transmission efficiency, the ideas of SW multiplexing functions have been explored. 18-20 There, the SW beams can flow along the shared waveguides and then divide into different output channels, which can be guided by a locally-generated magnetic field 18, 19, the global bias magnetic field along different orientations or the controlled coupling between two proximate homogeneous waveguides. 5, 21, 22 In electronics for parallel computation, FDMs enable the synchronous transmission of the signals encoded at different frequencies. Although this technique has been widely applied in microwave engineering and fiber optics, 23, 24 it remains to be realized in magnonic systems, despite several earlier preliminary demonstrations. In these designs, the FDM functions were enabled by the exploitation of the high anisotropy of the SWs dispersion relations.

SWs with a specific frequency in the magnetic waveguide can reach their highest intensity near the ferromagnetic resonant (FMR) field. 29-32 Similarly, the waveguide under a specific magnetic field support the SWs near the FMR frequency to reach to the highest intensity. In addition, it has been predicted<sup>33</sup> that a permalloy (Py, Ni<sub>81</sub>Fe<sub>19</sub>) microstructures can inhomogeneously magnetize the laterally proximate yttrium iron garnet (YIG, Y<sub>3</sub>Fe<sub>5</sub>O<sub>12</sub>) microstripe due to its much higher saturation magnetization  $(M_{\rm s})$ . The edge-localized SWs in YIG microstripe can thus be tuned by such mechanism. However, the edge-localized SWs can hardly be detected in YIG microstripes because they are spatially confined in an extremely narrow region.<sup>34, 35</sup> In this work, the SW FDM function is observed in YIG magnetic microstripe magnetized under a magnetic field gradient induced by a proximate Py microstripe (see Fig. 1). The SWs carrying the information are located in the central region of the YIG microstripe, which can be detected by micro-focused Brillouin light scattering ( $\mu$ -BLS). We demonstrate that two SWs with different frequencies can propagate simultaneously, separately and independently at different regions in the YIG microstripe. In addition, this technique provides a noninvasive mean to engineer the SW propagation without introducing an additional interface and related damping to YIG, which is advantageous compared with the recent developments of SW manipulation with interfacial exchange. 36-41 Our results implicate a potential approach for efficient FDM applications involving shared and integrated magnonic waveguides.

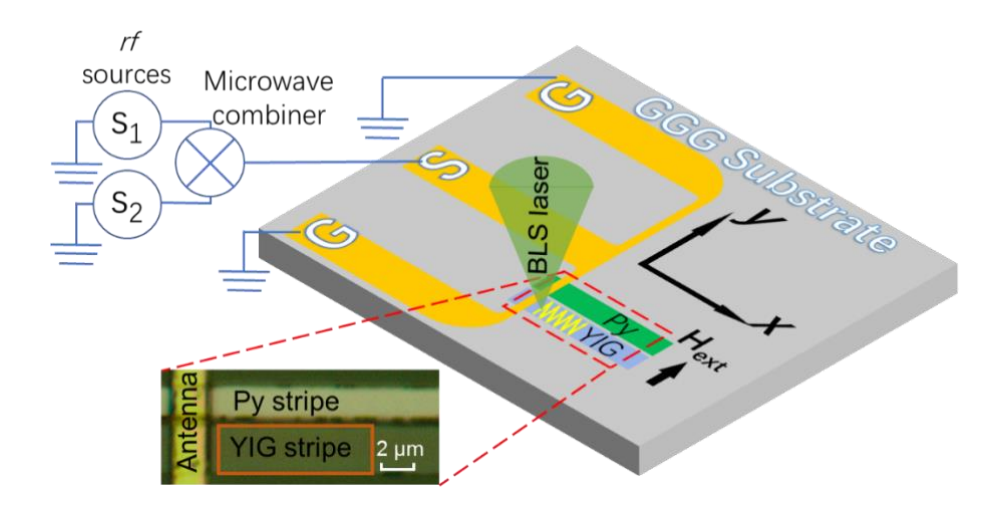


Fig. 1 Schematic illustration of the device layout and the experimental setup. The inset shows an optical microscopy image of the device indicated in the red dash box. The spin wave patterns were imaged in the region as indicated in red box.

Fig. 1 shows the schematic illustration of the device layout and the experimental setup. The 75-nm thick YIG and Py films were deposit by magnetron sputtering on single crystal gadolinium gallium garnet (GGG) substrates of 500- $\mu$ m thickness with (111) orientation. The 3- $\mu$ m wide YIG and 2- $\mu$ m wide Py microstripes were defined by using multi-step electron-beam lithography with highly accurate alignment and fabricated by the lift-off technique. The gap between them is 200 nm. Broadband ferromagnetic resonance of the thin films yields the  $4\pi M_s$  values of 9760 G and 1960 G, and damping factors ( $\alpha$ ) of  $7.3\times10^{-3}$  and  $2.1\times10^{-4}$  for Py and YIG films, respectively. For the excitation of the spin waves, the shortened end of a coplanar waveguide made of Ti(20 nm)/Au(500 nm) with a width approximately 2  $\mu$ m was placed on top of the microstripes. More details on the fabrication process were described in Ref. <sup>29</sup>.

Two microwave generators (Anritsu MG3697C and Berkeley Nucleonics Model 845) were used to excite SWs with different frequencies simultaneously. The output signals from the two generators were combined through a microwave splitter (Anaren Model 42100). The resultant signal from the mixer was then applied to the antenna structure. The external magnetic field ( $H_{\rm ext}$ ) was in-plane perpendicular to the stripe and was fixed at 680 Oe, corresponding to the Damon-Eshbach modes of the SWs. <sup>42</sup> All the observations of the spin waves were performed using  $\mu$ -BLS<sup>43</sup> with a laser wavelength of 532 nm.

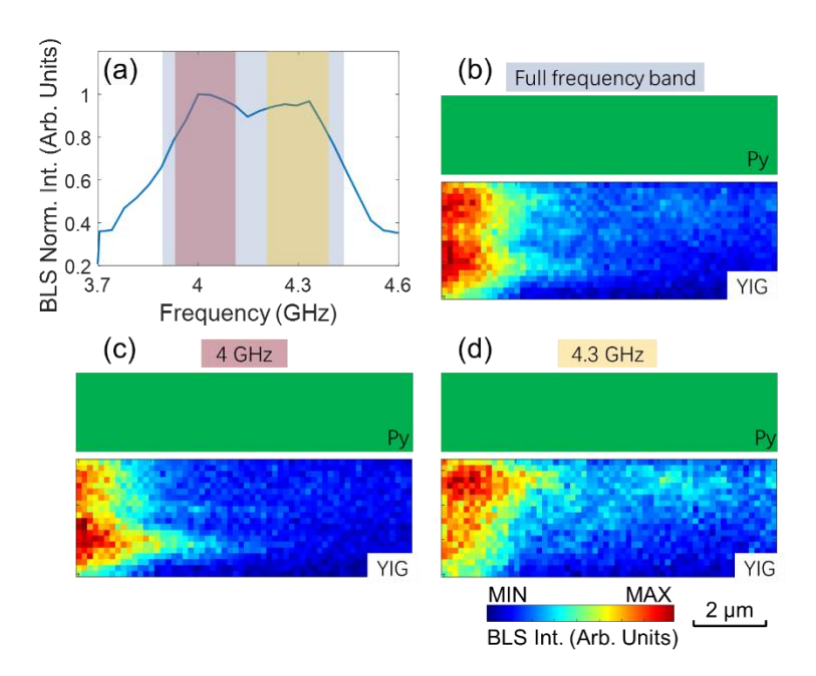


Fig. 2 Experimental demonstration of the prototype SW FDM function: (a) normalized BLS frequency spectrum recorded under the simultaneous excitations of 4 and 4.3 GHz. The spatial BLS intensity of the YIG microstripe with a proximate Py microstripe (green, same hereinafter) integrated (b) in the full frequency band (the grey region in (a)), (c) around 4 GHz (the pink region) and (d) around 4.3 GHz (the yellow region).

We measured the SWs in the YIG microstripe under the simultaneous excitations of 4 and 4.3 GHz. Here, the frequencies of 4 and 4.3 GHz were chosen according to the dispersion relations of the Damon-Eshbach SWs, whose intensities are maximized at frequencies a little higher than the FMR frequency.<sup>29</sup> In this study, the FMR frequency is  $f_0 = \gamma (H_0(H_0 + 4\pi M_s))^{0.5} \approx 3.8$  GHz at  $H_0 = 680$  Oe, where  $\gamma$  is the gyromagnetic ratio (2.8 MHz/Oe). The frequency separation of 0.3 GHz is chosen mainly because of the limitation of the BLS frequency resolution. If the band gap is narrower, the two peaks can be hard to distinguish in BLS spectra, considering the experimental linewidth of the peaks. The BLS intensity spectra at every measured position are integrated and normalized as shown in Fig. 2 (a). The two peaks around 4 and 4.3 GHz indicate that the majority of the SWs in the YIG microstripe are at the two frequencies. The intensity pattern of the propagating SWs integrated in the full frequency band [the grey region in Fig. 2 (a)] was mapped as shown in Fig. 2 (b). It shows that two SW beams emit from the antenna simultaneously. One is further away from the Py microstripe, while the other is closer to the Py microstripe. The intensity patterns integrated around 4 and 4.3 GHz [the pink region and the yellow region in Fig. 2 (a)] were mapped as shown in Fig. 2 (c) and 2(d), respectively. They reveal that the frequency of the SW beam farther away from (closer to) Py microstripe is 4 GHz (4.3 GHz). Neglecting the weaker intensity at the far end of the microstripe, the superposition of the two patterns in Fig. 2(c) and 2(d) can nicely match the pattern in Fig. 2 (b). Notice that the beams of the two SWs are gradually separated as they propagate toward the far end. And the patterns in both Fig. 2(b) and Fig. 2(d) contain zigzag shapes.

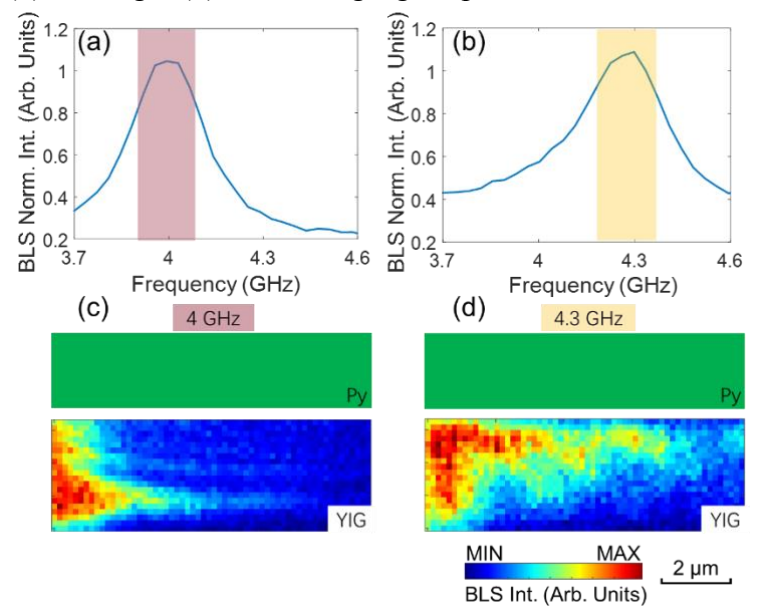


Fig. 3 Normalized BLS frequency spectrum recorded under the single excitation of (a) 4 and (b) 4.3 GHz. The pattern of the BLS intensity integrated around (c) 4 GHz (pink region in (a)) and (d) 4.3 GHz (yellow region in (b)) in the YIG microstripe under the single excitation.

To investigate the interactions between the two SWs, we measured the BLS intensity patterns with only one frequency excitation and compared them with the patterns under simultaneous excitations. The BLS intensity spectra at every measured position under a single excitation of 4 and 4.3 GHz are integrated and normalized as

shown in Fig. 3(a) and 3(b), respectively. The patterns of the BLS intensity integrated around 4 GHz [pink region in Fig. 3(a)] and 4.3 GHz [yellow region in Fig. 3(b)] are shown in Fig. 3(c) and 3(d), respectively. Their spatial SW profiles reproduce the results in Figs. 2(c) and 2(d), which means the two SW propagations in Fig. 2(b) do not interact with each other. We observe that the shapes of the patterns are similar with those under the simultaneous excitation [Fig. 2(c) and 2(d)]. Moreover, the increase of the intensities at the far end of the patterns in Fig. 3(c) and 3(d) is due to the decrease of the unwanted tail-like signal near the antenna compared with those under the simultaneous excitation, then the contrast at the far end increases. The similar shapes of the patterns indicate that the interactions between the two spin waves, such as the interference<sup>44</sup> or magnon scattering,<sup>45</sup> are negligible, because these interactions can generate additional signals or change the SWs patterns. Despite the output power of P = +20 dBm, the final power reaching the sample is significantly reduced due to the insertion of the combiner. Therefore the resultant BLS pattern in Fig. 2(b) is almost the linear superposition of the two spin waves in the YIG microstripe.<sup>46</sup>

The above results suggest that the FDM function can be potentially realized in the YIG microstripe with a proximate Py microstripe: the two SW beams can simultaneously propagate in the YIG microstripe; their channels are spatially separated at different positions; their propagations do not interact with each other. In a previous work,<sup>31</sup> it has been observed that the edge-localized SW beams can be shifted toward the center region of the microstripe with the increase of the frequency. This kind of shift is due to the higher  $H_{\text{eff}}$  in the center of the microstripe. To get a better understanding of the FDM mechanism, we performed micromagnetic simulations to study the  $H_{\rm eff}$ using Mumax3.47 The simulated Heff across the YIG microstripe versus its width at  $H_{\rm ext}$  = 680 Oe is plotted in Fig. 4 (a). The Py microstripe introduces an additional static dipolar field that inhomogeneously magnetizes the YIG microstripe. In the previous study<sup>33</sup>, the static dipolar field intensity was demonstrated to be inversely proportional to the distance. Fig. 4 (b) shows the experimentally acquired BLS intensities under different excitation frequencies in a range from 3.8 to 4.6 GHz across the YIG microstripe. The position in the YIG microstripe at which the measurement was performed is indicated by the orange dash line in the inset of Fig. 4 (a). The  $H_{\rm eff}$  in the YIG microstripe closer to Py is dramatically increased, resulting in the higher frequency of the propagating SWs. In addition, the frequency band of the SWs closer to the Py microstripe is wider than that far away from Py microstripe. This observation might be attributed to a wider  $H_{\rm eff}$  range as shown in the cyan patch of Fig. 4 (a). Moreover, it has been demonstrated that the wavelength of the SWs at a specific frequency changes with the variation of the magnetic field. 48, 49 Therefore, for the SWs propagating in the region with a wide  $H_{\rm eff}$  range, they might contain multiple wavelength components. Then the zig-zag patterns of the 4.3 GHz SWs in Fig. 2 (d) and Fig. 3 (d) can be understood by the interference between the components with different wavelengths. Here, it should be noted that the 4 and 4.3 GHz SWs do not interfere with each other. While the 4.3 GHz SWs contain a set of components with different wavelengths, their coherent interference with each other lead to the stable zig-zag patterns.<sup>29, 50, 51</sup> In addition, the dipolar coupling between the two waveguides might also lead to zig-zagshaped SW paths,  $^{5, 21, 22, 52}$  but due to the significantly different  $M_s$  of the Py and YIG, the coupling between the two microstripes is suppressed. In contrast, the 4 GHz SWs propagate in the region with relatively homogeneous  $H_{\text{eff}}$ . They have comparable single and monochromic wavelength component and appear with a straight decay pattern. Furthermore, in this study, the 4 and 4.3 GHz SWs were clearly divided under  $H_{\text{ext}} = 680$  Oe. Another pair of SWs at different frequencies are also supposed to be divided if the field is tuned accordingly. Besides, the tunability can be continuous if the field is tuned continuously.

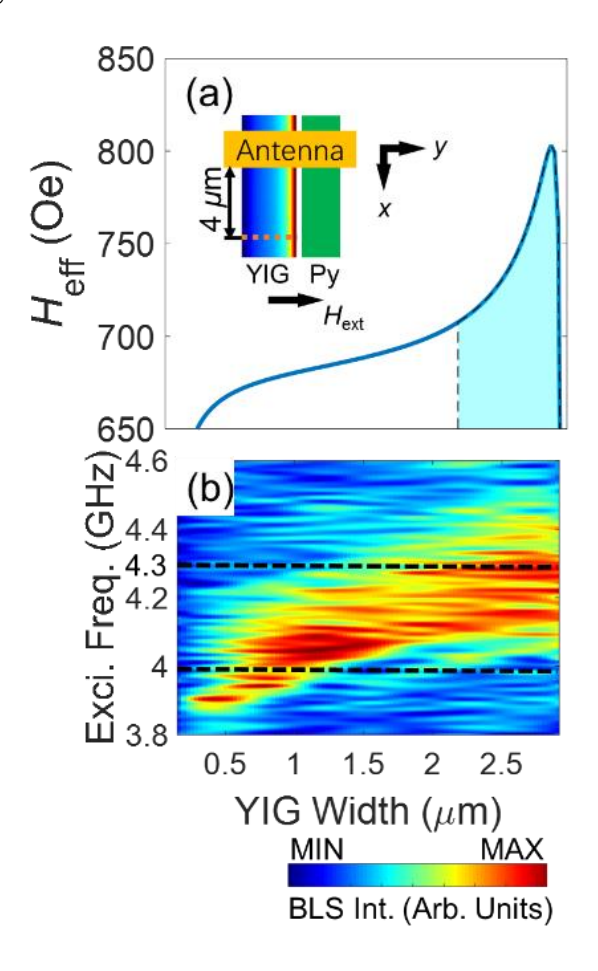


Fig. 4 (a) Simulated  $H_{\rm eff}$  across the YIG microstripe with a proximate Py microstripe under 680 Oe field. The  $H_{\rm eff}$  in the blue patched part is significantly increased due to the presence of the Py microstripe. Inset shows the schematic of the magnetic structure. The colormap encodes the y component of the  $H_{\rm eff}$  distribution inside the YIG microstripe. (b) Color coded BLS intensity at  $H_{\rm ext}$  = 680 Oe under different excitation frequencies in a range from 3.8 to 4.6 GHz across the YIG microstripe at the position indicated as the orange dash line in the inset of (a). The horizontal black dash lines indicate the 4 and 4.3 GHz excitation frequencies used in the spatial mapping.

It should be noted that in a single YIG magnonic waveguide, the  $H_{\rm eff}$  is inhomogeneous and symmetric across the width due to demagnetizing effects. Therefore the waveguide supports the symmetric propagation of edge-localized SWs, as well as the waveguide SWs with different frequencies. Nevertheless, the two kinds of SWs are very close to each other. Even though the edge region of YIG microstripe

can support the propagation edge-localized SWs in a broad frequency range, the edge region is narrow due to the weak  $M_s$  of YIG. On the other hand, the Py waveguide has wider edge regions. Therefore, the edge-localized SW beams have comparable width to the ones in this work.<sup>31, 52</sup> However, the SWs with different frequencies are still difficult to be separated in the narrow edge-localized channels.

It also has to be pointed out that the output channels are important components in a complete FDM circuit or device, however, they were missing in the current proof-of-concept design. Considering the width of the SW beams, the output channels can be realized using two nano-sized receivers, such as spin transfer nano-oscillators.<sup>53</sup>

In summary, we observed the spin wave frequency domain multiplexing function in an YIG microstripe with a laterally proximate permalloy (Py) stripe, which introduces an inhomogeneous dipolar magnetic field in the YIG microstripe. SWs with different frequencies can propagate simultaneously, separately and independently in different channels in such magnetic microstripe. The lower (higher) frequency SWs propagate along the side farther away from (closer to) the Py microstripe. A wide field range of the  $H_{\rm eff}$  variation on the side closer to the Py microstripe results in a wider SW frequency band and multiple wavelengths for SWs at a specific frequency. The zig-zag patterns might appear due to the interference of the SWs with multiple wavelengths. These results show a new method to divide the SWs with different frequencies hybridized in a signal waveguide. The FDM function can also be continuously tunable if the field can be varied continuously. This paves a way toward the parallel processing and transmission of data encoded in SWs .

\*nieyan@hust.edu.cn †novosad@anl.gov

## Acknowledgments

All work was performed at the Argonne National Laboratory and supported by the Department of Energy, Office of Science, Materials Science and Engineering Division. The use of the Centre for Nanoscale Materials was supported by the US. Department of Energy (DOE), Office of Sciences, Basic Energy Sciences (BES), under Contract No. DE-AC02-06CH11357.

ZZ acknowledges additional financial support from the China Scholarship Council (no. 201706160146) for a research stay at Argonne. J H acknowledges financial support from the Conselho Nacional de Desenvolvimento Científico e Tecnológico(CNPq)-Brasil. W Z acknowledges support from AFOSR under Grant no. FA9550-19-1-0254. M B J acknowledges support from US National Science Foundation under Grant No. 1833000.

- 1. R. L. Freeman, *Fundamentals of telecommunications*. (Wiley Online Library, 2005).
- 2. A. V. Chumak, V. I. Vasyuchka, A. A. Serga and B. Hillebrands, Nature Physics 11 (6) (2015).

- 3. M. Krawczyk and D. Grundler, Journal of Physics: Condensed Matter **26** (12), 123202 (2014).
- 4. A. Haldar, D. Kumar and A. O. Adeyeye, Nat Nano 11 (5), 437-443 (2016).
- 5. Q. Wang, P. Pirro, R. Verba, A. Slavin, B. Hillebrands and A. V. Chumak, Science Advances 4 (1) (2018).
- 6. A. V. Sadovnikov, A. A. Grachev, S. E. Sheshukova, Y. P. Sharaevskii, A. A. Serdobintsev, D. M. Mitin and S. A. Nikitov, Physical Review Letters **120** (25), 257203 (2018).
- 7. A. V. Sadovnikov, E. N. Beginin, S. E. Sheshukova, Y. P. Sharaevskii, A. I. Stognij, N. N. Novitski, V. K. Sakharov, Y. V. Khivintsev and S. A. Nikitov, Physical Review B **99** (5), 054424 (2019).
- 8. T. Schneider, A. A. Serga, B. Leven, B. Hillebrands, R. L. Stamps and M. P. Kostylev, Applied Physics Letters **92** (2), 022505 (2008).
- 9. A. A. Nikitin, A. B. Ustinov, A. A. Semenov, A. V. Chumak, A. A. Serga, V. I. Vasyuchka, E. Lähderanta, B. A. Kalinikos and B. Hillebrands, Applied Physics Letters **106** (10), 102405 (2015).
- 10. T. Fischer, M. Kewenig, D. A. Bozhko, A. A. Serga, I. I. Syvorotka, F. Ciubotaru, C. Adelmann, B. Hillebrands and A. V. Chumak, Applied Physics Letters **110** (15), 152401 (2017).
- 11. S. Klingler, P. Pirro, T. Brächer, B. Leven, B. Hillebrands and A. V. Chumak, Applied Physics Letters **105** (15), 152410 (2014).
- 12. B. Lenk, H. Ulrichs, F. Garbs and M. Münzenberg, Physics Reports **507** (4–5), 107-136 (2011).
- 13. G. Csaba, A. Papp and W. Porod, Journal of Applied Physics **115** (17), 17C741 (2014).
- 14. K.-S. Lee and S.-K. Kim, Journal of Applied Physics **104** (5), 053909 (2008).
- 15. N. Sato, K. Sekiguchi and Y. Nozaki, Applied Physics Express 6 (6), 063001 (2013).
- 16. G. Csaba, Á. Papp and W. Porod, Physics Letters A **381** (17), 1471-1476 (2017).
- 17. A. Khitun, Journal of Applied Physics 111 (5), 054307 (2012).
- 18. K. Vogt, F. Y. Fradin, J. E. Pearson, T. Sebastian, S. D. Bader, B. Hillebrands, A. Hoffmann and H. Schultheiss, Nature Communications **5**, 3727 (2014).
- 19. F. Heussner, A. A. Serga, T. Brächer, B. Hillebrands and P. Pirro, Applied Physics Letters **111** (12), 122401 (2017).
- 20. C. S. Davies, A. V. Sadovnikov, S. V. Grishin, Y. P. Sharaevsky, S. A. Nikitov and V. V. Kruglyak, IEEE Transactions on Magnetics **51** (11), 1-4 (2015).
- 21. A. Sadovnikov, E. Beginin, S. Sheshukova, D. Romanenko, Y. P. Sharaevskii and S. Nikitov, Applied Physics Letters **107** (20), 202405 (2015).
- 22. A. V. Sadovnikov, A. A. Grachev, E. N. Beginin, S. E. Sheshukova, Y. P. Sharaevskii and S. A. Nikitov, Physical Review Applied 7 (1), 014013 (2017).
- 23. H. Ishio, J. Minowa and K. Nosu, Journal of Lightwave Technology **2** (4), 448-463 (1984).
- 24. N. Michailow, M. Matthé, I. S. Gaspar, A. N. Caldevilla, L. L. Mendes, A. Festag and G. Fettweis, IEEE Transactions on Communications **62** (9), 3045-3061 (2014).
- 25. A. V. Sadovnikov, V. A. Gubanov, S. E. Sheshukova, Y. P. Sharaevskii and S. A.

- Nikitov, Physical Review Applied 9 (5), 051002 (2018).
- 26. A. V. Sadovnikov, E. N. Beginin, S. A. Odincov, S. E. Sheshukova, Y. P. Sharaevskii, A. I. Stognij and S. A. Nikitov, Applied Physics Letters **108** (17), 172411 (2016).
- 27. F. Heussner, M. Nabinger, T. Fischer, T. Brächer, A. A. Serga, B. Hillebrands and P. Pirro, physica status solidi (RRL) Rapid Research Letters **12** (12), 1800409 (2018).
- 28. F. Heussner, G. Talmelli, M. Geilen, B. Heinz, T. Brächer, T. Meyer, F. Ciubotaru,
- C. Adelmann, K. Yamamoto and A. A. Serga, arXiv preprint arXiv:1904.12744 (2019).
- 29. Z. Zhang, M. Vogel, J. Holanda, J. Ding, M. B. Jungfleisch, Y. Li, J. E. Pearson, R. Divan, W. Zhang, A. Hoffmann, Y. Nie and V. Novosad, Physical Review B **100** (1), 014429 (2019).
- 30. V. E. Demidov, S. Urazhdin, A. Zholud, A. V. Sadovnikov and S. O. Demokritov, Applied Physics Letters **106** (2), 022403 (2015).
- 31. V. E. Demidov, S. O. Demokritov, K. Rott, P. Krzysteczko and G. Reiss, Applied Physics Letters **92** (23), 232503 (2008).
- 32. R. O. Cunha, J. Holanda, L. H. Vilela-Leão, A. Azevedo, R. L. Rodríguez-Suárez and S. M. Rezende, Applied Physics Letters **106** (19), 192403 (2015).
- 33. Z. Zhang, M. Vogel, M. B. Jungfleisch, A. Hoffmann, Y. Nie and V. Novosad, arXiv preprint arXiv:1907.06718 (2019).
- 34. S. Li, W. Zhang, J. Ding, J. E. Pearson, V. Novosad and A. Hoffmann, Nanoscale **8** (1), 388-394 (2016).
- 35. P. Pirro, T. Brächer, A. V. Chumak, B. Lägel, C. Dubs, O. Surzhenko, P. Görnert, B. Leven and B. Hillebrands, Applied Physics Letters **104** (1), 012402 (2014).
- 36. S. Klingler, V. Amin, S. Geprägs, K. Ganzhorn, H. Maier-Flaig, M. Althammer, H. Huebl, R. Gross, R. D. McMichael, M. D. Stiles, S. T. B. Goennenwein and M. Weiler, Physical Review Letters **120** (12), 127201 (2018).
- 37. J. Chen, C. Liu, T. Liu, Y. Xiao, K. Xia, G. E. W. Bauer, M. Wu and H. Yu, Physical Review Letters **120** (21), 217202 (2018).
- 38. H. Qin, S. J. Hämäläinen and S. van Dijken, Scientific Reports 8 (1), 5755 (2018).
- 39. C. Liu, J. Chen, T. Liu, F. Heimbach, H. Yu, Y. Xiao, J. Hu, M. Liu, H. Chang, T. Stueckler, S. Tu, Y. Zhang, Y. Zhang, P. Gao, Z. Liao, D. Yu, K. Xia, N. Lei, W. Zhao and M. Wu, Nature Communications 9 (1), 738 (2018).
- 40. K. An, V. S. Bhat, M. Mruczkiewicz, C. Dubs and D. Grundler, Physical Review Applied 11 (3), 034065 (2019).
- 41. Y. Li, W. Cao, V. P. Amin, Z. Zhang, J. Gibbons, J. Sklenar, J. Pearson, H. Paul, S. Mark, B. William, V. Novosad, A. Hoffmann and W. Zhang, (2019).
- 42. R. W. Damon and J. R. Eshbach, Journal of Physics and Chemistry of Solids **19** (3), 308-320 (1961).
- 43. T. Sebastian, K. Schultheiss, B. Obry, B. Hillebrands and H. Schultheiss, Frontiers in Physics **3** (35) (2015).
- 44. P. Pirro, T. Brächer, K. Vogt, B. Obry, H. Schultheiss, B. Leven and B. Hillebrands, physica status solidi (b) **248** (10), 2404-2408 (2011).
- 45. A. V. Chumak, A. A. Serga and B. Hillebrands, Nature Communications 5, 4700 (2014).

- 46. K. Livesey, in *Handbook of Surface Science*, edited by R. E. Camley, Z. Celinski and R. L. Stamps (North-Holland, 2015), Vol. 5, pp. 169-214.
- 47. A. Vansteenkiste, J. Leliaert, M. Dvornik, M. Helsen, F. Garcia-Sanchez and B. Van Waeyenberge, AIP Advances 4 (10), 107133 (2014).
- 48. K. Vogt, H. Schultheiss, S. J. Hermsdoerfer, P. Pirro, A. A. Serga and B. Hillebrands, Applied Physics Letters **95** (18), 182508 (2009).
- 49. V. E. Demidov, S. Urazhdin and S. O. Demokritov, Applied Physics Letters **95** (26), 262509 (2009).
- 50. O. Buttner, M. Bauer, C. Mathieu, S. O. Demokritov, B. Hillebrands, P. A. Kolodin, M. P. Kostylev, S. Sure, H. Dotsch, V. Grimalsky, Y. Rapoport and A. N. Slavin, IEEE Transactions on Magnetics **34** (4), 1381-1383 (1998).
- 51. P. Clausen, K. Vogt, H. Schultheiss, S. Schäfer, B. Obry, G. Wolf, P. Pirro, B. Leven and B. Hillebrands, Applied Physics Letters **99** (16), 162505 (2011).
- 52. V. E. Demidov, J. Jersch, S. O. Demokritov, K. Rott, P. Krzysteczko and G. Reiss, Physical Review B **79** (5), 054417 (2009).
- 53. M. R. Pufall, W. H. Rippard, S. E. Russek, S. Kaka and J. A. Katine, Physical Review Letters **97** (8), 087206 (2006).